The Astrophysical Journal, 579:261–269, 2002 November 1
© 2002. The American Astronomical Society. All rights reserved. Printed in U.S.A.

1.65 MICRON (*H* BAND) SURFACE PHOTOMETRY OF GALAXIES. X. STRUCTURAL AND DYNAMICAL PROPERTIES OF ELLIPTICAL GALAXIES

Stefano Zibetti[1]
Max-Planck-Institut für Astrophysik, Karl-Schwarzschild-Strasse 1, D-85741 Garching bei München, Germany; zibetti@mpa-garching.mpg.de

Giuseppe Gavazzi
Università degli Studi di Milano-Bicocca, Piazza delle Scienze 3, I-20126 Milan, Italy

Marco Scodeggio and Paolo Franzetti[1]
Istituto di Fisica Cosmica "G. Occhialini," CNR, via Bassini 15, I-20133 Milan, Italy

and

Alessandro Boselli
Laboratoire d'Astrophysique de Marseille, Traverse du Siphon, F-13376 Marseille Cedex 12, France
Received 2002 May 3; accepted 2002 July 8

ABSTRACT

We analyze the structural and dynamical properties of a sample of 324 nearby elliptical and dwarf elliptical galaxies observed during an extensive near-IR survey in the *H* band (1.65 μm). The fundamental plane is determined and a significant tilt is assessed. The origins of such a tilt are investigated by means of a spherically symmetric, isotropic, pressure-supported dynamical model relying on the observed surface brightness profiles. The systematic variation of the shape coefficient converting the measured central velocity dispersion σ_0 into the virial rms velocity $\sigma_{\rm rms}$ is found to be the main cause of the tilt, due to aperture effects. Moreover, the ratio between the dynamical mass $M_{\rm dyn}$ and the total *H*-band luminosity L_H turns out to be roughly constant along the luminosity sequence of ellipticals: *H*-band luminosity is therefore a reliable and cheap estimator of the dynamical mass of the E galaxies.

Subject headings: galaxies: elliptical and lenticular, cD — galaxies: fundamental parameters — galaxies: photometry — infrared: galaxies

1. INTRODUCTION

The assumption that normal galaxies are in dynamical equilibrium implies that, for a given type of dynamics (i.e., rotation or pressure supported), the dynamical status of the system is strongly related to its mass distribution. Using the further assumption that the mass inside the "observable" radius of a galaxy is traced by the (stellar) light, the dynamical parameters should be, at least in first approximation, determined by the structural parameters describing the light distribution. In the case of elliptical galaxies, these systems have been proved to be mainly pressure supported, and the fundamental dynamical parameter is the central velocity dispersion σ_0. The simplest way of describing the light distribution of a galaxy is to measure the half-light (or effective) radius R_e and the average surface brightness I_e inside R_e. If the elliptical galaxies formed a homologous family, both from the structural and the dynamical point of view, and the M/L ratio were constant, the virial theorem would imply a linear relation between the logarithm of the three parameters given by

$$\log R_e = 2\log\sigma_0 - \log I_e + k\ . \qquad (1)$$

A linear relation has actually been found (the fundamental plane [FP]; Djorgovski & Davis 1987; Dressler et al. 1987), but the coefficients differ significantly from those predicted by the virial theorem (this is known as the "tilt" of the FP). This implies the nonconstancy of M/L and/or the breaking of the homology. However, the existence of the FP as a tight relation requires that the variations of M/L or the breaking of the homology happen in a very systematic way.

Most of the early studies devoted to this problem assumed homology and concluded that a systematic increase of M/L with luminosity is needed both in optical (e.g., Bender, Burstein, & Faber 1992) and in near-IR (NIR) passbands (e.g., Pahre, de Carvalho, & Djorgovski 1998). However, many studies in which the surface brightness profiles are analyzed both in optical (e.g., Djorgovski, Davis, & Kent 1985; Schombert 1986, 1987; Jedrzejewski 1987; de Carvalho & da Costa 1988; Capaccioli, Piotto, & Rampazzo 1988) and in NIR passbands (e.g., Gavazzi et al. 2001; Scodeggio et al. 2002) have found systematic variations of the profile shape and concentration index (i.e., the structural parameter quantifying how much the light distribution is centrally peaked)[2] among elliptical galaxies, implying a breaking of the homology. In pioneering work, Prugniel & Simien (1997) and Graham & Colless (1997) produced evidence in favor of a strong influence of structural nonhomology on the tilt of the FP. Busarello et al. (1997) concluded that most of the tilt could be accounted for by dynamical

[1] Università degli Studi di Milano-Bicocca, Piazza delle Scienze 3, I-20126 Milan, Italy.

[2] Many definitions of the concentration index have been proposed in the literature; the definition hereafter adopted is $c_{31} = r_{75}/r_{25}$, the ratio between the radii enclosing 75% and 25% of the total luminosity of the galaxy (see Gavazzi et al. 2001; Scodeggio et al. 2002).

nonhomology, although spatial nonhomology and stellar population effects can give significant contributions as well. More recently, Bertin, Ciotti, & Del Principe (2002) showed how the departure from spatial homology contributes to the tilt of the FP in the B band for a small sample of nearby E galaxies imaged with high signal-to-noise ratio (S/N).

The claim by Scodeggio et al. (1998) that the amount of tilt is significantly lower in the NIR bands than in the optical ones implies, however, a significant role of different stellar populations (age, metallicity) in determining the M/L and the structural parameters. NIR passbands are the most suitable for studying the structural parameters because they trace much better than visible passbands the bulk of the luminous mass of the galaxies that sits in old stellar populations. Moreover, they are less sensitive to dust obscuration and line blanketing, and in turn this reduces the age/metallicity effects on the M/L ratio. We have performed a systematic and extensive investigation of the structural properties in the H (K') band for a sample of nearby galaxies, covering all the morphological types and extending from high to low luminosities, i.e., to the dwarf regime (see Gavazzi et al. 2000a, 2001, and references therein). Based on these surface brightness profiles, Scodeggio et al. (2002) demonstrate a systematic relationship between the concentration index c_{31} and the total H-band luminosity that is almost completely independent of the eye-ball morphological classification: from this relationship the structural nonhomology of the elliptical family can be inferred. The structural and dynamical properties of the whole sample of surveyed galaxies are analyzed by Pierini et al. (2002), adopting the κ-space formalism (Bender et al. 1992).

In this paper we present a study of the relationships between the structural H-band (1.65 μm) properties of 324 elliptical and dwarf elliptical galaxies. The relationships with dynamical parameters are analyzed for a subsample of 135 galaxies ranging from the highest luminosities to the dwarf regime and extending the original sample of 73 galaxies studied by Scodeggio et al. (1998). The sample is described in § 2. In § 3 we study the Kormendy relation between the effective surface brightness μ_e and the effective radius R_e. In § 4 a derivation of the H-band FP is presented using different fitting methods, while an analysis of the contribution to the FP tilt due to M/L and homology breaking is performed in § 5 using a simple dynamical model relying on the measured surface brightness profiles. The method, independently developed by Zibetti (2001), is very similar to that of Bertin et al. (2002). It should be stressed, however, that we analyzed a 10 times larger sample using NIR photometric data, as opposed to the B-band data analyzed by Bertin et al. (2002). A brief discussion and the conclusions of this work are given in §§ 6 and 7.

2. THE SAMPLE

In this paper we analyze the photometric H-band (1.65 μm) structural parameters of a sample of 324 bona fide elliptical and dwarf elliptical galaxies selected among members of five nearby rich clusters, namely, the Virgo, Coma, A1367, A262, and Cancer clusters, in addition to a significant population of galaxies in the "Great Wall," the bridge between Coma and A1367. Observations and photometric analysis of this sample are reported by Gavazzi et al. (2000a, 2000b, and references therein). The total H-band luminosity L_H, the effective radius R_e (i.e., the radius enclosing half of the total luminosity), the effective surface brightness μ_e, defined as the average surface brightness within R_e, and the concentration index c_{31} are derived from the azimuthally averaged surface photometry (see Gavazzi et al. 2000a). Absolute luminosities and physical radii are calculated attributing to each galaxy the mean cluster ("cloud") distance, with the exception of the galaxies in the Great Wall, for which the redshift distance $H_0 = 75\ \mathrm{km\ s^{-1}\ Mpc^{-1}}$ is assumed. For a subsample of 135 galaxies, dynamical analysis could be performed relying on central velocity dispersion measures (σ_0) obtained from the literature (see Scodeggio et al. 1998 and references therein). The entire sample comprises 274 ellipticals (129 with σ_0 measurements) and 50 dwarf ellipticals/spheroidals (six with σ_0 measurements).

Details on the sample completeness in the Coma Supercluster region ($11^{\mathrm{h}}30^{\mathrm{m}} \leq \alpha \leq 13^{\mathrm{h}}30^{\mathrm{m}}$, $18^\circ \leq \delta \leq 32^\circ$) and the Virgo Cluster are given in Table 1: for each bin of photographic magnitude m_{pg} and $\log L_{H_\odot}$, the total number of galaxies in the Catalogue of Galaxies and of Clusters of Galaxies (Zwicky et al. 1961–1968; $m_{\mathrm{pg}} < 15.7$)—for the Coma region—and in the Virgo Cluster Catalog (Binggeli, Sandage, & Tammann 1985)—for the Virgo cluster—are given, along with the total number and percentage of galaxies in the photometric sample and in the dynamical sample. In translating m_{pg} into $\log L_{H_\odot}$, an average color-luminosity relation of $B-H = 0.3 \log L_{H_\odot} + 0.5$ is assumed (see Scodeggio et al. 2002). A mean distance modulus of 34.9 is assumed for the Coma region, while a distance of 17 Mpc is attributed to the Virgo A Cluster, according to Gavazzi et al. (1999). As far as the photometric parameters are concerned, we cover a representative sample comprising the transition between the giant—and the dwarf—regime. Dynamical measurements are available only for giants, with few exceptions providing some hints on the behavior of the scaling relations at low luminosity.

3. THE KORMENDY RELATION

The Kormendy relation (Kormendy 1985) between the effective surface brightness μ_e and the effective radius R_e is shown in Figure 1. Filled circles represent giant elliptical galaxies, open circles dwarfs. The dotted lines indicate isoluminosity loci, assuming a mean ellipticity of 0.35, from 10^8 to $10^{12}\ L_{H_\odot}$. Giant ellipticals follow a mean relation given by $\mu_e = (2.84 \pm 0.06) \log R_e + (15.65 \pm 0.03)$. This is obtained from an orthogonal least-squares bivariate (OLSB) fitting procedure with 3 σ rejection and is represented in Figure 1 by the solid line. Dispersion is noticeable: 0.62 mag arcsec^{-2}. The slope [-0.88 ± 0.02 expressed in $\log(L_{H_\odot}\ \mathrm{kpc}^{-2})/\log(\mathrm{kpc})$] is consistent with -0.83 ± 0.08 as measured by Kormendy & Djorgovski (1989) in the R band.

Low-luminosity and dwarf elliptical galaxies do not follow the same relationship as giants: the latter would imply that galaxies at lower luminosity should be increasingly compact, M32-like objects, while observations show that the lower luminosity of dwarfs is mainly due to their lower surface brightness. However, from Figure 1 no clear dichotomy can be assessed between giants and dwarfs, and it could be argued that, to a first approximation, galaxies populate uniformly the μ_e-R_e space, avoiding the region below the mean Kormendy relation. In other words, for each effective radius there is an upper limiting effective surface brightness, and this is lower for larger radii.

TABLE 1
COMPLETENESS FOR THE COMA SUPERCLUSTER AND THE VIRGO CLUSTER

				PHOTOMETRIC		DYNAMIC	
REGION	m_{pg}	$\log L_{H_\odot}$	TOTAL NUMBER	Number	Percent	Number	Percent
Coma.....	<15.7	>10.5	186	180	97	86	46
Virgo.....	<14	>9.6	35	31	89	25	71
	14–15	9.6–9.1	72	36	50	7	10
	15–16	9.1–8.7	99	12	12	2	2
	16–18	8.7–7.8	304	6	2	0	0

4. THE FUNDAMENTAL PLANE RELATION

In this section we present a study of the fundamental plane relationship between R_e, I_e (defined by $\log I_e/L_{H_\odot}$ kpc$^{-2} = 16.0 - 0.4\mu_e$), and the central velocity dispersion σ_0. This is described by

$$\log R_e = a \log \sigma_0 + b \log I_e + c \, . \quad (2)$$

Many methods are available for inferring the values of a, b, and c. We have considered the orthogonal error-weighted (OEW) and the measurement errors and intrinsic scatter three-dimensional (MIST; see La Barbera, Busarello, & Capaccioli 2000) fitting procedures. The OEW method (developed by M. Scodeggio, S. Zibetti, and P. Franzetti) is based on the minimization of the error-weighted distance of the measured points from the plane. Details on the mathematical treatment and a full description of the method are given in Appendix A. The MIST method requires an a priori determination of the covariance matrix for error and intrinsic scatter. The first one has been estimated as the mean error covariance matrix for the sample. Lacking any reliable model for the intrinsic scatter, the correspondent covariance matrix has been defined null. We consider the results for a number of different fitting procedures and parameters and, separately, for the whole dynamical sample (135 galaxies) and for the subsample of 120 galaxies having $\sigma_0 > 100$ km s^{-1}:[3] they are presented in Table 2 and in Figures 2*a*–2*b*. The columns in Table 2 are as follows: (1) fitting method (MIST or OEW); (2) type of MIST fit (bisector [BIS] or using $\log R_e$ as a dependent variable [Y3]); (3) error correlation for $\log I_e$-$\log R_e$ (if "Yes," $\sigma^2_{\log R_e \log I_e} \sim 0.015 \sim 1.2\sigma_{\log R_e}\sigma_{\log I_e}$ is assumed; if "No," errors on $\log I_e$ and $\log R_e$ are considered uncorrelated);[4] (4) lower limit on σ_0 (km s^{-1}); (5)–(6) a and associated 1 σ (68.3% confidence level) error; (7)–(8) b and associated 1 σ (68.3% confidence level) error.

Inferred parameters a and b show very large inconsistencies in the case of the MIST fit, depending on the sample selection, the error correlations, and the type of fit (bisector or with an individual dependent variable). On the other hand, OEW fits are more stable and consistent within the error limits. This is illustrated in Figures 2*a*–2*b*. The distribution of $\Delta\chi^2(a, b)$ with respect to the minimum (marked by a plus sign) is represented in logarithmic gray scale for the OEW+correlation fit on the whole sample (Fig. 2*a*) and on the sample having $\sigma_0 > 100$ km s^{-1} (Fig. 2*b*). Confidence levels of 68.3%, 95.4%, 99.0%, and 99.99% are shown as superposed contour lines. Superposed symbols mark best MIST fits for BIS with error correlation (*crosses*), Y3 with error correlation (*diamonds*), BIS without correlation

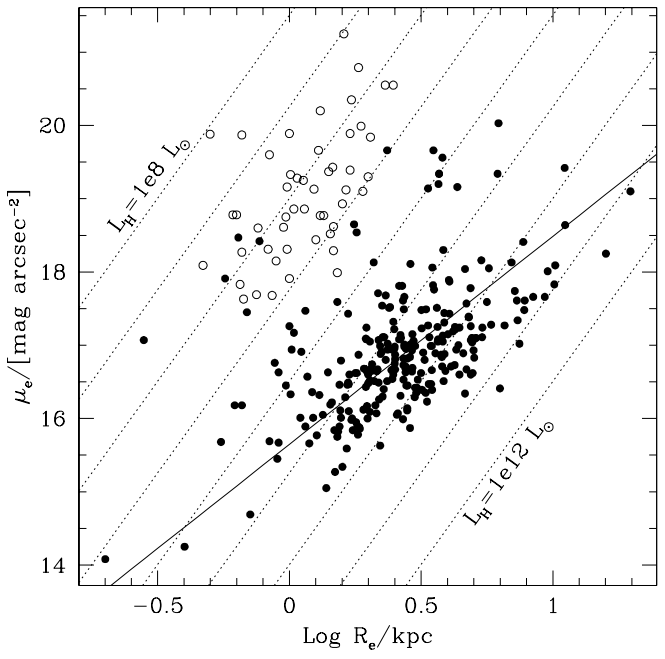

FIG. 1.—Kormendy relation. *Filled circles*: Giant elliptical galaxies; *open circles*: dwarfs; *dotted lines*: isoluminosity lines, assuming mean ellipticity 0.35, in 0.5 dex intervals; *solid line*: the OLSB fit for the giants.

[3] Values of $\sigma_0 < 100$ km s^{-1} are usually affected by noticeable uncertainties.

[4] This is the case if the photometric calibration error is the main source of uncertainty on $\log I_e$.

TABLE 2
FIT PARAMETERS

Fitting Method (1)	Type (2)	Correlation (3)	σ_0 (4)	a (5)	Error (6)	b (7)	Error (8)
MIST.....	BIS	Yes	0	1.20	0.11	−0.87	0.04
MIST.....	Y3	Yes	0	1.56	0.13	−1.09	0.08
MIST.....	BIS	No	0	1.37	0.09	−0.86	0.04
MIST.....	Y3	No	0	1.42	0.10	−0.89	0.06
MIST.....	BIS	Yes	100	0.56	0.12	−0.95	0.05
MIST.....	Y3	Yes	100	1.47	0.15	−1.19	0.10
MIST.....	BIS	No	100	1.13	0.12	−0.91	0.04
MIST.....	Y3	No	100	1.40	0.12	−0.98	0.06
OEW.....	...	Yes	0	1.46	0.1	−0.83	0.07
OEW.....	...	No	0	1.47	0.1	−0.84	0.07
OEW.....	...	Yes	100	1.38	0.1	−0.88	0.07
OEW.....	...	No	100	1.41	0.1	−0.87	0.07

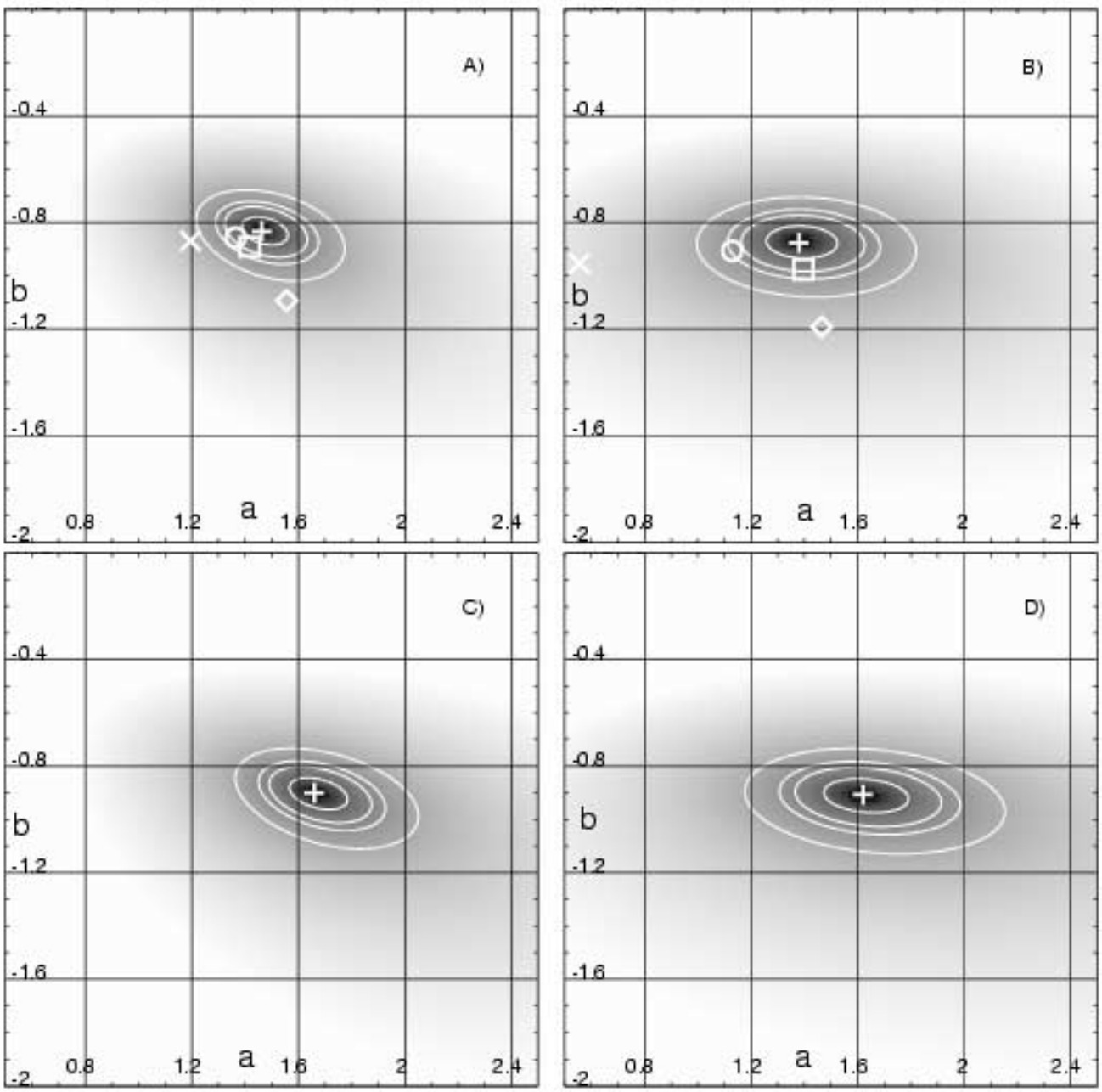

FIG. 2.—The $\Delta\chi^2(a,\ b)$ distribution with respect to the minimum in logarithmic gray scale for the OEW+correlation fit (*a*) on the whole sample and (*b*) on the sample having $\sigma_0 > 100$ km s^{-1}. Minimum is marked by a plus sign. Confidence levels of 68.3%, 95.4%, 99.0%, and 99.99% are shown as superposed contour lines. Superposed symbols in (*a*) and (*b*) mark best MIST fits for BIS with error correlation (*crosses*), Y3 with error correlation (*diamonds*), BIS without correlation (*circles*) and Y3 without correlation (*squares*). (*c–d*) Same as (*a*) and (*b*), respectively, but using velocity dispersions obtained by the dynamical model (see § 5.1) in the hypothesis of constant $M/L = 1$.

(*circles*), and Y3 without correlation (*squares*). MIST fit results are substantially inconsistent with the OEW results as well, being inside the 95.4% confidence level at best and outside the 99.99% confidence level when error correlation is considered. These inconsistencies are probably due to the high sensitivity of the MIST algorithms to the error and intrinsic scatter model, which is ill determined.

As our best estimate of the fundamental plane in the H passband, we adopt the OEW fit with error correlation as applied to the $\sigma_0 > 100$ km s^{-1} limited sample:

$$\log R_e = (1.38 \pm 0.1) \log \sigma_0 - (0.88 \pm 0.07) \log I_e + 5.47 \ . \quad (3)$$

In Figure 3 we show the $\log R_e$ distribution along the fitted plane. The average dispersion is 0.14, which is somewhat higher than the average 1 σ error associated with $\log R_e$ (0.09). We conclude that intrinsic scatter is present in the FP relation.

5. ORIGINS OF THE FUNDAMENTAL PLANE TILT

The zeroth-order interpretation of the origins of the FP relationship is derived applying virial equilibrium and the hypothesis that elliptical galaxies form a homological family with respect to their structural and dynamical parameters.

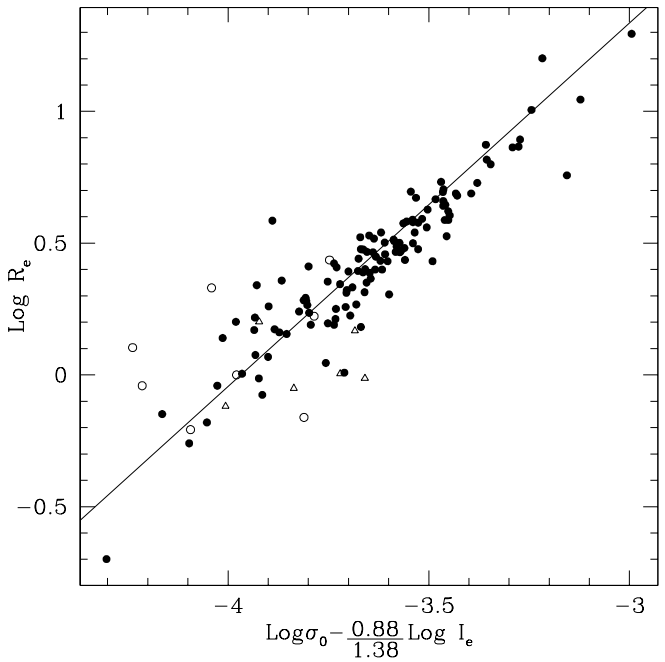

FIG. 3.—FP section showing $\log R_e$ distribution along the fitted plane. *Triangles*: Dwarf galaxies; *circles*: giants. *Open symbols*: Galaxies having $\sigma_0 < 100$ km s^{-1}. Typical error bars are 0.09 dex along $\log R_e$ axis and 0.10 dex along the x-axis.

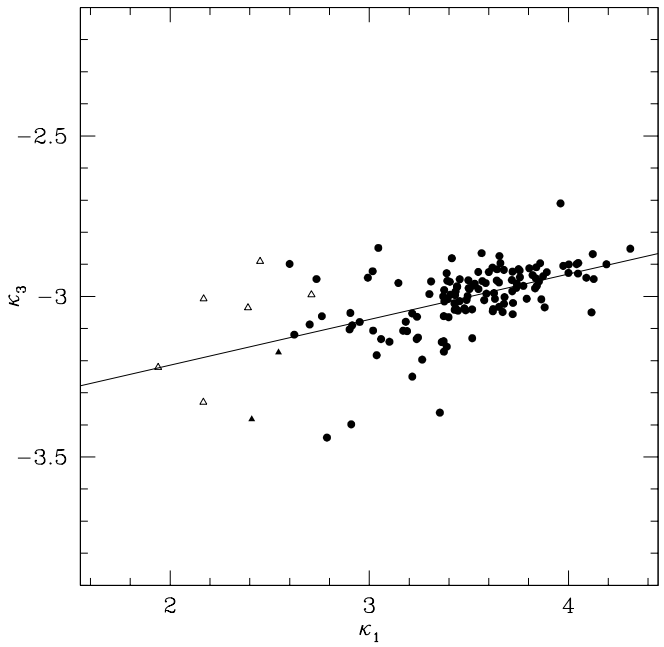

FIG. 4.—The κ_3-κ_1 projection. *Triangles*: Dwarf galaxies; *circles*: giants. *Open symbols*: Galaxies having $\sigma_0 < 100$ km s^{-1}. *Solid line*: Best least-squares fit ($\kappa_3 = 0.14\kappa_1 - 3.50$).

This implies

$$M\frac{1}{R_g} \propto \langle v^2 \rangle, \quad R_g \equiv \frac{GM^2}{U} \ , \tag{4}$$

$$M \propto \frac{M}{L} I_e R_e^2 \ , \tag{5}$$

$$R_g \propto R_e \ , \tag{6}$$

$$\langle v^2 \rangle \propto \sigma_0^2 \ , \tag{7}$$

where M is the total mass, R_g is the gravitational radius, $\langle v^2 \rangle$ is the mean squared velocity of the "particles" (i.e., the stars), G is the gravitational constant, and U is the total gravitational potential energy. So the expected equation for the fundamental plane is

$$\log R_e = 2\log\sigma_0 - \log I_e - \log\frac{M}{L} + k \ , \tag{8}$$

where the k-constant includes all the "shape coefficients" used for translating the observed quantities into the virial ones, as well as the unit conversion factors. According to the homological hypothesis, the difference between the measured coefficients and the expected ones (the so called tilt of the FP) is entirely produced by a systematic change in M/L along the galaxy luminosity sequence. This is shown for our sample in Figure 4, using the κ-space formalism (Bender et al. 1992) where

$$\kappa_1 = \left(\log\sigma_0^2 + \log R_e\right)/\sqrt{2} \propto \log M \ , \tag{9}$$

$$\kappa_3 = \left(\log\sigma_0^2 - \log\Sigma_e - \log R_e\right)/\sqrt{3} \propto \log\frac{M}{L} \ . \tag{10}$$

A systematic increase in M/L with mass is found, in agreement with the claims of Bender et al. (1992) in the B band and Pahre et al. (1998) in the K band. However, the analysis of surface brightness profiles of elliptical galaxies performed in different passbands by many authors during the last years (for the H band see Gavazzi et al. 2001; Scodeggio et al. 2002) demonstrated a systematic change in the profile shapes with luminosity and/or radii, requiring some deviation from pure homology. Systematic variations of the k-term in equation (8) have to be taken into account, and κ_3 no longer represents a trend of M/L but results from a combination of M/L and shape coefficient effects. In order to disentangle the two contributions, we developed the model described in the next section.

5.1. *Dynamical Model*

We model elliptical galaxies as spherically symmetric, isotropic, pressure-supported dynamical systems. Deviations from spherical symmetry and the contribution of rotation to the kinetic energy are neglected (see Ciotti & Lanzoni 1997). M/L is left as a free parameter but is assumed to be constant within each galaxy. The radial light density profile is derived by deprojection of the measured azimuthally averaged surface brightness profile. This is translated into the mass density profile assuming an initial guess value for M/L of 1.0 (solar units). Solving the hydrostatical equilibrium equation, the velocity dispersion profile is obtained. The contribution to the Doppler line broadening of each mass element is integrated along the line of sight within a characteristic slit aperture to obtain the model central velocity dispersion $\sigma_{0m} = \sigma_{0m}(M/L)$. M/L is then adjusted to match the measured σ_0. It is worth noticing here that the computed values of σ_0 are influenced both by the intrinsic nonhomology of the galaxies (i.e., different shapes of mass distribution profiles) and by the aperture effects, because of the different fraction of the galaxy light that contributes to the line broadening inside the slit aperture.

Details on the mathematical treatment are given in Appendix B.

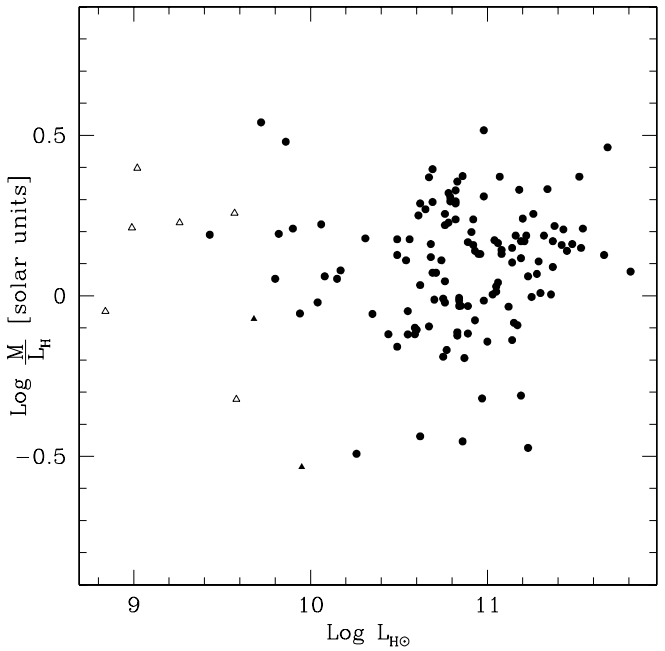

FIG. 5.—M/L ratios as derived from the model as a function of the total H-band luminosity. Symbols as in Fig. 4.

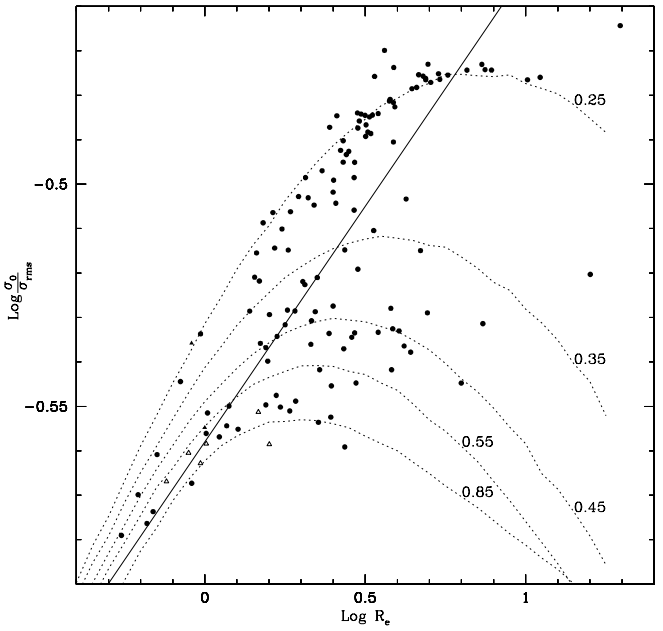

FIG. 6.—The $\sigma_0/\sigma_{\rm rms}$ ratio as a function of R_e. Symbols as in Fig. 4. *Solid line*: OLSB fit. *Dashed lines*: Theoretically expected relation for families of homologous galaxies modeled by Sérsic laws. Each curve is labeled with the corresponding ν index.

5.2. *M/L Ratios*

Unlike in the case of the κ_3 coefficient, the values that we derive here for M/L are not influenced by the varying shape of the surface brightness profiles and by the aperture effects.

In Figure 5 $\log M/L$ is shown as a function of the total H-band luminosity. No significant evidence of systematic variation of M/L with L can be seen. The average $\log M/L$ is 0.09 (corresponding to $M/L \sim 1.2$), with a large dispersion of 0.2 dex. Systematic variations of M/L are therefore unlikely to be solely responsible for the tilt of the FP. Further evidence comes from replacing the measured values of σ_0 with those obtained from the model assuming a constant M/L for all galaxies:[5] the resulting distribution of $\Delta\chi^2(a, b)$ is shown in Figures 2*c* and 2*d* for the whole dynamical sample and for the subsample with $\sigma_0 > 100$ km s^{-1}, respectively. In both cases the distribution is inconsistent with the values $a = 2$, $b = -1$ expected on the basis of the virial theorem and homology. This demonstrates that the observed deviations of the profiles from self-similarity are expected to cause an FP tilt similar to that observed, in the absence of any variation in M/L.

5.3. *Homology Breaking and Aperture Effects*

The dynamical model provides the phase-space density distribution for each galaxy. Potential and kinetic energy can be calculated, and the gravitational radius R_g (see eq. [B7]) and the rms velocity $\langle v^2\rangle^{1/2} \equiv \sigma_{\rm rms}$ can be determined as well. In order to investigate the consequences of the breaking of the homology and of the aperture effects on the coefficients of the FP relation, we study the dependence of the ratios $\sigma_0/\sigma_{\rm rms}$ and R_e/R_g on R_e. R_e/R_g does not show any significant correlation with R_e. The relation between $\sigma_0/\sigma_{\rm rms}$ and R_e is shown in Figure 6.

The clear correlation observed between these two parameters demonstrates that the commonly assumed linear proportionality between σ_0 and $\sigma_{\rm rms}$ (eq. [7]) does not hold. In principle, this can be a consequence both of an aperture effect, depending on the slit aperture relative to R_e, and of the different velocity dispersion profiles.

The OLSB fit for the points gives

$$\log\frac{\sigma_0}{\sigma_{\rm rms}} = 0.106\log R_e - 0.558 \qquad (11)$$

and is shown as the solid line. The dashed lines superposed on Figure 6 show the theoretically expected aperture effect for homologous galaxies following the Sérsic law[6] (Sérsic 1968) with index $\nu = 0.25$, 0.35, 0.45, 0.55, and 0.85. Each curve reflects the dependence of the velocity dispersion on the radius and presents a linearly increasing part, whose slope is largely independent of ν, followed by a maximum and a decreasing part, whose location and slope strongly depend on ν. It is evident that the slope of the mean relation is largely determined by the aperture effect in its linear part, while the nonhomology of the light profiles (given by the different ν indexes) mostly contributes to the scatter. Inserting the average relation in the virial FP equation (8), the FP coefficients $a = 1.65$ and $b = 0.83$ are obtained. Such values are in very good agreement (within the 68.3% confidence level) with those obtained fitting the FP on the data sample in which σ_0 was replaced by the central velocity dispersion modeled assuming constant M/L (see Figs. 2*c*–2*d*). The agreement with the "real" FP coefficients is worse, although within the 99.99% confidence level (see Figs. 2*a*–2*b*).

[5] The exact value of M/L is irrelevant in order to obtain the a and b coefficients. $M/L = 1.0$ has been assumed for simplicity.

[6] $I(r) = I_0\exp[-(r/a)^\nu]$, where I_0 is the central surface brightness, ν is the index ($\nu = 0.25$ corresponding to a de Vaucouleurs profile, $\nu = 1$ to an exponential), and a is the scale factor.

6. DISCUSSION

The analysis performed in § 4 confirms the existence of the FP relation in the NIR H band claimed by Scodeggio et al. (1998). The inconsistencies between the plane coefficients obtained applying different fitting techniques stresses the fact that comparison between different FP determinations has to be done using homogeneous fitting methods and, in any case, using large samples of galaxies. Because of its stability, irrespective of different hypotheses on the covariance matrix, the OEW fit appears to be the most reliable one.

Our determination of the FP in the H passband ($a = 1.38 \pm 0.1$, $b = -0.88 \pm 0.07$, $c = 5.47$; see Fig. 2) is consistent within 1 σ with that obtained by Scodeggio et al. (1998) using a subsample of 73 of our galaxies in the Coma Cluster and with that obtained by Pahre et al. (1998) in the K band with a slightly different fitting method. In our analysis we did not apply any correction for the sample incompleteness bias. The method used to calculate such corrections (see Scodeggio et al. 1998 and references therein) relies on Monte Carlo simulations to generate a synthetic sample of galaxies reproducing the observed relations between the galaxy luminosity and the observable quantities involved in the FP. However, such relations are very poorly determined when extended to the faint objects, and this affects severely the reliability of the bias corrections. Moreover, although the present sample represents a significant extension of the one considered by Scodeggio et al. (1998) toward low luminosities, we find that the values of the FP coefficients determined in the present work are closer to the uncorrected ($a = 1.51 \pm 0.09$, $b = -0.80 \pm 0.03$) than to the corrected ($a = 1.66 \pm 0.10$, $b = -0.85 \pm 0.03$) ones in Scodeggio et al. (1998), thus indicating that the assumptions underlying the bias correction may be incorrect.

Applying a dynamical model to the measured surface brightness profiles, the resulting FP tilt and its origins have been studied. This model represents a higher order approximation than that given by the homological hypothesis, since the shape coefficients translating the measured parameters into the virial ones are allowed to vary according to the observed surface brightness profile. Only two assumptions on the structure and dynamics are made:

1. M/L is constrained to be homogeneous within each galaxy and
2. spherical symmetry and isotropic velocity dispersion are assumed.

Real galaxies are actually much more complex systems; nevertheless, it is worth noticing that discrepancies from this description are not likely to affect our conclusions considerably. The use of NIR passband photometry minimizes the variation of M/L due to different stellar populations. Moreover, Ciotti & Lanzoni (1997) showed that asymmetry and anisotropy affect only slightly the kinetic energy in elliptical galaxies modeled according to Sérsic profiles.

Contrary to the results of Pahre et al. (1998) in the K band and of several authors in optical passbands (e.g., Bender et al. 1992), the M/L ratio estimated on the basis of our dynamical model in the H band does not show any significant increase with luminosity. The H-band luminosity appears to be a good first-order estimator for the dynamical mass of elliptical galaxies, in analogy to the claim by Gavazzi, Pierini, & Boselli (1996), who found direct proportionality between the H-band luminosity and dynamical mass for disk systems.

In turn, the constancy of M/L implies that the tilt of the FP ($\sim 56°$) is mainly caused by a systematic variation in the laws that translate the observed parameters into the virial ones. In fact, we found that the ratio R_e/R_g does not present any systematic variation (spatial homology holds), while the ratio $\sigma_0/\sigma_{\rm rms}$ increases with increasing R_e. As demonstrated in § 5.3, this is mainly a consequence of the aperture effects, which are strictly related to the way σ_0 is measured, rather than of structural nonhomology. The systematic variation of $\sigma_0/\sigma_{\rm rms}$ can entirely account for the tilt of the synthetic FP ($\sim 53°$) in which σ_0 has been computed from the model assuming constant M/L. Moreover, this leads to the conclusion that the kinetic energy scales approximately as $\sigma_0^{1.65}$ instead of σ_0^2, in agreement with the claim of Busarello et al. (1997). However, some residual systematic variation of M/L and R_e/R_g is required to account for the tilt of the measured FP.

The analysis performed by Bertin et al. (2002) by applying a similar dynamical model on a sample of 14 galaxies observed in the B-band concluded that although no strict homology holds for the elliptical galaxies, a nonnegligible contribution from M/L variation is needed to account for the tilt of the FP in the B band. However, no aperture effects are considered in this work, and this in turn could lead to overestimating the contribution due to the M/L variation. The tilt has been proved to increase at shorter wavelengths (see Scodeggio et al. 1998; Pahre et al. 1998). In principle this could be due either to systematic variations of the global M/L ratio at the shorter optical wavelengths or to the different way in which the aperture effects and nonhomology act with respect to the NIR passbands, e.g., due to color gradients. However, Scodeggio et al. (2002) showed that the color-magnitude relation $B-H$ versus H for the elliptical galaxies is very flat. Given the constancy of M/L in the H band, this in turn rules out large variations of global M/L as a main cause of the increased tilt of FP at shorter wavelengths. The influence of the aperture effects and of the profile shapes on the tilt in the optical B and V bands will be analyzed in a forthcoming paper.

The tightness of the FP relation shows that the causes of the tilt, whatever they are, should act while preserving a structural and dynamical continuity along the sequence of ellipticals. The structural continuity between the giant and the dwarf regime is confirmed also by the Kormendy projection of the FP (see § 3). An important point emerging from the R_e-μ_e distribution is the existence of a cutoff in the effective surface brightness: the upper limit in surface brightness decreases with increasing effective radius, with the same slope of the Kormendy relation for giants.

7. SUMMARY AND CONCLUSIONS

We have determined the fundamental plane of elliptical galaxies in nearby rich clusters (mainly Virgo and Coma) in the NIR H passband. Our result may be written $\log R_e = (1.38 \pm 0.1) \log \sigma_0 - (0.88 \pm 0.07) \log I_e + 5.47$.

The relation is tight, showing a dispersion of 0.14 dex in R_e, while typical errors are 0.09 dex. The origins of the tilt of the fitted plane with respect to the virial predictions for a homologous family of galaxies have been investigated by means of a simple dynamical model. Spherical symmetry,

hydrodynamical equilibrium, and isotropic velocity dispersion are assumed. Constant M/L within each galaxy has been assumed as a free parameter and used to calculate density and velocity dispersion profiles. M/L was then adjusted in order to match predicted values of σ_0 with the measured ones.

The obtained values of M/L do not show any dependence on the total luminosity. Systematic variations of M/L are then ruled out as the main cause of the tilt of the fundamental plane. We showed that the ratio between the rms velocity and the central velocity dispersion is systematically varying as a function of R_e, mainly because of the different slit aperture relative to R_e in the spectroscopic measurement of σ_0. This variation is responsible for most of the amount of the tilt.

The constancy of M/L makes the H-band total luminosity a reliable and cheap first-order estimator for the dynamical mass of elliptical galaxies. This matches the analogous claim by Gavazzi et al. (1996) for disk galaxies.

Applying the dynamical model to data sets extended to low-luminosity and dwarf elliptical galaxies, which will become available in the future, will provide crucial information in order to determine whether the hypotheses of constant M/L and pure isotropic pressure support can describe (at least in first approximation) the whole family of elliptical galaxies. The structural continuity between the giant and the dwarf regime is shown by the distribution of galaxies in the μ_e-R_e plane. The existence of an upper limit to the effective surface brightness has been found that follows the classical Kormendy relation for the giants.

We thank Gianni Busarello and Francesco La Barbera for kindly providing the MIST code and for helpful advice, and Simon D. M. White for useful discussion.

APPENDIX A

ORTHOGONAL ERROR-WEIGHTED FIT

The orthogonal error-weighted fit minimizes the orthogonal χ^2, defined by the sum of the squared distances from the fitted plane, weighted on the errors. This gives

$$\chi^2 = \Sigma_i \frac{d^2(i)}{\delta_d^2} \ , \tag{A1}$$

where distances are defined by

$$d(i) = \sqrt{\frac{[a \log \sigma_0(i) + b \log I_e(i) + c - \log R_e(i)]^2}{1 + a^2 + b^2}} \tag{A2}$$

and the corresponding errors are

$$\delta_d = \sqrt{\frac{a^2\delta_{\sigma_0}^2 + b^2\delta_{I_e}^2 + \delta_{R_e}^2 - 2b\delta_{I_e}\delta_{R_e}r}{1 + a^2 + b^2}} \ . \tag{A3}$$

In the last equation δ_{σ_0}, δ_{I_e}, and δ_{R_e} are the errors on the logarithm of the corresponding quantities, and r is the error correlation factor between $\log I_e$ and $\log R_e$ (see § 3). The minimum is approached using a Powell algorithm (see Press et al. 1992) starting from an initial guess value in the three-space of the FP coefficients obtained combining the linear fits on the three projections of the plane.

APPENDIX B

THE DYNAMICAL MODEL

The dynamical model adopted in this paper for the elliptical galaxies assumes

1. spherical symmetry,
2. an isotropic velocity dispersion tensor,
3. hydrostatic equilibrium, and
4. a homogeneous M/L ratio throughout the galaxy.

The light density distribution $\nu(r)$ is obtained by deprojecting the azimuthally averaged surface brightness profile via the inversion of the Abel integral (Binney & Tremaine 1987, eq. [4.58a]):

$$\nu(r) = -\frac{1}{\pi}\int_r^\infty \frac{dI(R)}{dR}\frac{dR}{\sqrt{R^2 - r^2}} \ . \tag{B1}$$

Because of the inconsistencies (negative light density) induced by irregularities and slope inversions in the empirical profiles, these are replaced in the calculations by the profiles fitted according to analytical laws: de Vaucouleurs ($r^{1/4}$; de Vaucouleurs 1948), exponential, bicomponent (exponential+exponential or exponential+de Vaucouleurs), and exponentially truncated de Vaucouleurs or exponential (see Gavazzi et al. 2000a, 2001 for details).

Assuming an initial guess value for the M/L ratio, the mass density profile is obtained:

$$\rho(r) = \frac{M}{L}\nu(r) \ . \tag{B2}$$

For the isotropic dispersion tensor the equation for the hydrostatic equilibrium can be written

$$\frac{d}{dr}\left[\sigma_r^2(r)\rho(r)\right] = -\frac{GM(r)\rho(r)}{r^2} \ . \tag{B3}$$

By solving the latter, we obtain the radial velocity dispersion profile:

$$\sigma_r^2(r) = \frac{G}{\nu(r)}\frac{M}{L}\int_r^\infty \frac{L(r')\nu(r')dr'}{r'^2} \ . \tag{B4}$$

Typical dispersion profiles show a maximum that is more peaked and nearer the center the more cuspy the density profile is, in agreement with the claims by Binney (1980) and by Ciotti & Lanzoni (1997) for the de Vaucouleurs and different Sérsic profiles.

Integrating the light-weighted contributions to the Doppler line broadening inside a standard slit aperture (corresponding to $2'' \times 6''$ at the distance of Coma), the expected central velocity dispersion σ_{0m} is obtained. Since σ_{0m} goes as $(M/L)^{1/2}$, M/L is consequently adjusted in order to obtain $\sigma_{0m} = \sigma_0$ for the galaxies in the dynamical sample. For the other galaxies an average $M/L \sim 1.2$ is assumed.

Given the hypotheses above and the density and velocity dispersion profiles, the phase-space distribution function $f(\boldsymbol{r}, \boldsymbol{v})$ is completely determined and can be used to obtain the total gravitational potential energy

$$U = -4\pi\int_0^\infty r^2 dr \frac{GM(r)\rho(r)}{r} \tag{B5}$$

and the total kinetic energy

$$K = \int\int (\tfrac{1}{2}|\boldsymbol{v}|^2) f(\boldsymbol{r}, \boldsymbol{v}) d^3\boldsymbol{r} d^3\boldsymbol{v} \ . \tag{B6}$$

In turn, this yields

$$R_g = \frac{GM^2}{U} \ , \tag{B7}$$

$$\sigma_{\rm rms} \equiv \left\langle v^2 \right\rangle^{1/2} = \sqrt{2K/M} \ . \tag{B8}$$

All calculations are implemented numerically in a C code written by S. Zibetti relying on standard algorithms taken from Press et al. (1992). High numerical accuracy is obtained: the $K/|U|$ ratio differs from the expected virial value of $\frac{1}{2}$ by less than 10^{-4} at most.

REFERENCES

Bender, R., Burstein, D., & Faber, S. M. 1992, ApJ, 399, 462
Bertin, G., Ciotti, L., & Del Principe, M. 2002, A&A, 386, 149
Binggeli, B., Sandage, A., & Tammann, G. A. 1985, AJ, 90, 1681
Binney, J. 1980, MNRAS, 190, 873
Binney, J., & Tremaine, S. 1987, Galactic Dynamics (Princeton: Princeton Univ. Press)
Busarello, G., Capaccioli, M., Capozziello, S., Longo, G., & Puddu, E. 1997, A&A, 320, 415
Capaccioli, M., Piotto, G., & Rampazzo, R. 1988, AJ, 96, 487
Ciotti, L., & Lanzoni, B. 1997, A&A, 321, 724
de Carvalho, R. R., & da Costa, L. N. 1988, ApJS, 68, 173
de Vaucouleurs, G. 1948, Ann. d'Astrophys., 11, 247
Djorgovski, S., & Davis, M. 1987, ApJ, 313, 59
Djorgovski, S., Davis, M., & Kent, S. 1985, in New Aspects of Galaxy Photometry, ed. J.-L. Nieto (Lecture Notes in Physics 232; Berlin: Springer), 257
Dressler, A., Lynden-Bell, D., Burstein, D., Davies, R. L., Faber, S. M., Terlevich, R., & Wegner, G. 1987, ApJ, 313, 42
Gavazzi, G., Boselli, A., Scodeggio, M., Pierini, D., & Belsole, E. 1999, MNRAS, 304, 595
Gavazzi, G., Franzetti, P., Scodeggio, M., Boselli, A., & Pierini, D. 2000a, A&A, 361, 863
Gavazzi, G., Franzetti, P., Scodeggio, M., Boselli, A., Pierini, D., Baffa, C., Lisi, F., & Hunt, L. K. 2000b, A&AS, 142, 65
Gavazzi, G., Pierini, D., & Boselli, A. 1996, A&A, 312, 397
Gavazzi, G., Zibetti, S., Boselli, A., Franzetti, P., Scodeggio, M., & Martocchi, S. 2001, A&A, 372, 29
Graham, A., & Colless, M. 1997, MNRAS, 287, 221
Jedrzejewski, R. I. 1987, MNRAS, 226, 747
Kormendy, J. 1985, ApJ, 295, 73
Kormendy, J., & Djorgovski, S. 1989, ARA&A, 27, 235
La Barbera, F., Busarello, G., & Capaccioli, M. 2000, A&A, 362, 851
Pahre, M. A., de Carvalho, R. R., & Djorgovski, S. G. 1998, AJ, 116, 1606
Pierini, D., Gavazzi, G., Franzetti, P., Scodeggio, M., & Boselli, A. 2002, MNRAS, 332, 422
Press, W. H., Teukolsky, S. A., Vetterling, W. T., & Flannery, B. P. 1992, Numerical Recipes in C: The Art of Scientific Computing (2d ed.; Cambridge: Cambridge Univ. Press)
Prugniel, P., & Simien, F. 1997, A&A, 321, 111
Schombert, J. M. 1986, ApJS, 60, 603
———. 1987, ApJS, 64, 643
Scodeggio, M., Gavazzi, G., Belsole, E., Pierini, D., & Boselli, A. 1998, MNRAS, 301, 1001
Scodeggio, M., Gavazzi, G., Franzetti, P., Boselli, A., Zibetti, S., & Pierini, D. 2002, A&A, 384, 812
Sérsic, J. L. 1968, Atlas de Galaxias Australes (Córdoba: Obs. Astron., Univ. Nacional Córdoba)
Zibetti, S. 2001, M.S. thesis, Università degli Studi, Milano
Zwicky, F., Herzog, E., & Wild, P. 1961–1968, Catalogue of Galaxies and of Clusters of Galaxies (Pasadena: Caltech)